NRC·CNRC

NRC Publications Archive
Archives des publications du CNRC

Ultrasound-modulated optical imaging using a powerful long pulse laser

Rousseau, Guy; Blouin, Alain; Monchalin, Jean-Pierre

This publication could be one of several versions: author's original, accepted manuscript or the publisher's version. / La version de cette publication peut être l'une des suivantes : la version prépublication de l'auteur, la version acceptée du manuscrit ou la version de l'éditeur.
For the publisher's version, please access the DOI link below./ Pour consulter la version de l'éditeur, utilisez le lien DOI ci-dessous.

Publisher's version / Version de l'éditeur:
https://doi.org/10.1364/OE.16.012577
Optics Express, 16, 17, pp. 12577-12590, 2008

NRC Publications Record / Notice d'Archives des publications de CNRC:
https://nrc-publications.canada.ca/eng/view/object/?id=8e5d141b-8f88-4346-9343-b6d0b4e788a6
https://publications-cnrc.canada.ca/fra/voir/objet/?id=8e5d141b-8f88-4346-9343-b6d0b4e788a6

Access and use of this website and the material on it are subject to the Terms and Conditions set forth at
https://nrc-publications.canada.ca/eng/copyright
READ THESE TERMS AND CONDITIONS CAREFULLY BEFORE USING THIS WEBSITE.

L'accès à ce site Web et l'utilisation de son contenu sont assujettis aux conditions présentées dans le site
https://publications-cnrc.canada.ca/fra/droits
LISEZ CES CONDITIONS ATTENTIVEMENT AVANT D'UTILISER CE SITE WEB.

Questions? Contact the NRC Publications Archive team at PublicationsArchive-ArchivesPublications@nrc-cnrc.gc.ca. If you wish to email the authors directly, please see the first page of the publication for their contact information.

Vous avez des questions? Nous pouvons vous aider. Pour communiquer directement avec un auteur, consultez la première page de la revue dans laquelle son article a été publié afin de trouver ses coordonnées. Si vous n'arrivez pas à les repérer, communiquez avec nous à PublicationsArchive-ArchivesPublications@nrc-cnrc.gc.ca.

National Research Council Canada | Conseil national de recherches Canada

Canada

Ultrasound-modulated optical imaging using a powerful long pulse laser

Guy Rousseau, Alain Blouin, and Jean-Pierre Monchalin

Industrial Materials Institute, National Research Council of Canada, 75 de Mortagne Blvd., Boucherville, Québec, Canada, J4B 6Y4

guy.rousseau@cnrc-nrc.gc.ca

Abstract: Ultrasound-modulated optical imaging (or tomography) is an emerging biodiagnostic technique which provides the optical spectroscopic signature and the localization of an absorbing object embedded in a strongly scattering medium. We propose to improve the sensitivity of the technique by using a pulsed single-frequency laser to raise the optical peak power applied to the scattering medium and thereby collect more ultrasonically tagged photons. When the detection of tagged photons is done with a photorefractive interferometer, a pulsed laser enables to reduce the response time of the photorefractive crystal below the speckle decorrelation time. Results obtained with a GaAs photorefractive interferometer are presented for 30- and 60-mm thick scattering media.

©2008 Optical Society of America

OCIS codes: (170.1065) Acousto-optics; (170.3880) Medical and biological imaging; (170.7050) Turbid media; (120.1088) Adaptative interferometry; (120.3180) Interferometry

References and links

1. L. V. Wang and H. Wu, *Biomedical Optics: Principles and Imaging* (John Wiley and Sons, Hoboken, New Jersey, 2007).
2. L. Wang, S. L. Jacques, and X. Zhao, "Continuous-wave ultrasonic modulation of scattered laser light to image objects in turbid media," Opt. Lett. **20**, 629-631 (1995).
3. S. Lévêque, A. C. Boccara, M. Lebec, and H. Saint-Jalmes, "Ultrasonic tagging of photon paths in scattering media: parallel speckle modulation processing," Opt. Lett. **24**, 181-183 (1999).
4. M. Atlan, B. C. Forget, F. Ramaz, A. C. Boccara, and M. Gross, "Pulsed acousto-optic imaging in dynamic scattering media with heterodyne parallel speckle detection," Opt. Lett. **30**, 1360-1362 (2005).
5. S. Sakadzic and L. V. Wang, "High-resolution ultrasound-modulated optical tomography in biological tissues," Opt. Lett. **29**, 2770-2772 (2004).
6. T. W. Murray, L. Sui, G. Maguluri, R. A. Roy, A. Nieva, F. Blonigen, and Ch. A. DiMarzio, "Detection of ultrasound-modulated photons in diffuse media using the photorefractive effect," Opt. Lett. **29**, 2509-2511, (2004).
7. F. Ramaz, B. C. Forget, M. Atlan, A. C. Boccara, M. Gross, P. Delaye, and G. Roosen, "Photorefractive detection of tagged photons in ultrasound modulated optical tomography of thick biological tissues," Opt. Express **12**, 5469-5474 (2004), http://www.opticsinfobase.org/abstract.cfm?URI=oe-12-22-5469.
8. F. A. Duck, "Medical and non-medical protection standards for ultrasound and infrasound," Prog. Biophys. Molec. Biol. **93**, 176-191 (2007).
9. Laser Institute of America, *American National Standard for the Safe Use of Lasers ANSI Z136.1-2000* (ANSI, Orlando, Florida, 2000).
10. J.-P. Monchalin, "Optical detection of ultrasound at a distance using a confocal Fabry-Perot interferometer," Appl. Phys. Lett. **47**, 14-16 (1985).
11. A. Blouin and J.-P. Monchalin, "Detection of ultrasonic motion of a scattering surface by two-wave mixing in a photorefractive GaAs crystal," Appl. Phys. Lett. **65**, 932-934 (1994).
12. J.-P. Monchalin, "Optical detection of ultrasound," IEEE Trans. Ultrason. Ferroelectr. Freq. Control **33**, 485-499 (1986).
13. L. V. Wang, "Mechanisms of Ultrasonic Modulation of Multiply Scattered Coherent Light: An Analytic Model," Phys. Rev. Lett. **87**, 043903 (2001).
14. L. E. Kinsler and A. R. Frey, *Fundamentals of Acoustics* (John Wiley and Sons, New York, 1962).
15. J. Krautkrämer and H. Krautkrämer, *Ultrasonic Testing of Materials* (Springer-Verlag, New York, 1977).
16. D. Royer, N. Dubois, and M. Fink, "Optical probing of pulsed, focused ultrasonic fields using a heterodyne interferometer," Appl. Phys. Lett. **61**, 153-155 (1992)

17. W. A. Riley and W. R. Klein, "Piezo-optic coefficients of liquids," J. Acous. Soc. Am. **42**, 1258-1261 (1967).
18. G. M. Hale and M. R. Querry, "Optical constants of water in the 200-nm to 200-μm wavelength region," Appl. Opt. **12**, 555-563 (1973).
19. S. Prahl, "Optical absorption of water," http://omlc.ogi.edu/spectra/water/.
20. J. Li and L. V. Wang, "Image reconstruction in ultrasound-modulated optical tomography," Proc. SPIE **5320**, 268–272 (2004).

1. Introduction

Optical imaging techniques for biomedical diagnostics are currently very actively developed. These techniques have in particular the advantage of being based on non-ionizing radiation while being able to provide morphological as well as functional information [1]. Ultrasound-modulated optical imaging (or tomography) is an emerging technique which allows the localization of an optically absorbing object imbedded in an optically scattering medium through the detection of ultrasound-modulated photons [2-7]. This method combines the good spatial resolution (mm scale) and penetration depth (cm scale) of ultrasound waves with the spectroscopic information provided by photons. A practical limit to the use of this technique is its poor sensitivity or low signal-to-noise ratio. Even though the optical absorption of water is relatively low in the therapeutic window, the strong scattering of photons propagating in tissues reduces significantly the number of collectable photons. Moreover, for biomedical applications, safety considerations limit the power level of both the ultrasonic wave and the laser beam. The peak negative pressure of the ultrasonic wave must remain below a value prescribed by the so-called mechanical index (MI) to avoid cavitation and its side effects [8]. Similarly, the laser beam irradiance must be maintained below the maximum permissible exposure (MPE) to avoid heating damage [9].

In ultrasound-modulated imaging, the tagged photons can be detected by full field imaging of the speckle pattern with an array of detectors (CCD camera) [3,4] or by an interferometric scheme using a single photodetector [2,5-7]. Methods based on arrays of detectors require intensive data processing but provide a better signal-to-noise ratio [3-4]. The interferometric scheme is either based on a confocal Fabry-Perot interferometer [5,10] or on an adaptative photorefractive interferometer [6-7,11]. Both instruments present a large optical etendue when compared to conventional interferometers [12]. The adaptative photorefractive interferometer uses a photorefractive crystal to recombine the reference beam and the signal beam through a dynamic volume grating which replicates the wave front of the signal beam to that of the reference beam. This approach was developed for laser-ultrasonic non-destructive testing of materials where almost all the photons of the signal beam are modulated [11]. In ultrasound-modulated optical imaging, most photons in the signal beam are not modulated since the insonified zone in the scattering medium is generally much smaller than the illuminated zone. Moreover, an ultrasonic toneburst presents compression and rarefaction zones. Consequently, each scattered photon undergoes both positive and negative phase shifts, thereby acquiring a net phase modulation which is rather small [13].

A direct way to enhance the number of tagged photons is to increase the optical power incident on the scattering medium. However, to respect the maximum permissible exposure in terms of average power, the increase of the instantaneous power must be counterbalanced by a reduction of the exposure duration. This suggests the use of a train of pulses of high peak intensity with an appropriate duty cycle. In such a situation, the number of photons is high mainly for the relevant period of time, that is, during the transit time of the ultrasonic toneburst in the scattering medium. A laser pulse of high power density also shortens the response time of the dynamic hologram written in the crystal of the photorefractive interferometer. This is important to overcome the speckle decorrelation associated with mechanical vibrations and with tissue motions for in vivo applications. With a pulsed laser, a short response time is also essential to ensure the build-up of the dynamic hologram in a time shorter than the laser pulse duration.

In this paper, we describe an experiment based on the use of a long pulse single-frequency laser at $1.064\,\mu m$. Photons are tagged in 30- and 60-mm thick scattering media with ultrasonic tonebursts generated by a 4.35-MHz transducer. The tagged photons are detected with a quadratic response photorefractive interferometer using a GaAs crystal and characterized by a large optical etendue.

2. Experimental setup

The schematic diagram of the experimental setup used for the detection of the ultrasound-modulated photons is shown in Fig. 1. The beam of the single-frequency laser source (L) is separated by a beam splitter (BS) into a reference beam (R) and a signal beam (S). The signal beam is directed (along the axis y) toward the scattering medium (SM) which is locally insonified by an ultrasonic transducer (UT) emitting ultrasonic pulses which propagate along the axis z. Photons collected at the output of the scattering medium are sent together with the reference beam into a photorefractive interferometer (PRI) to detect the ultrasound-tagged photons as a function of time.

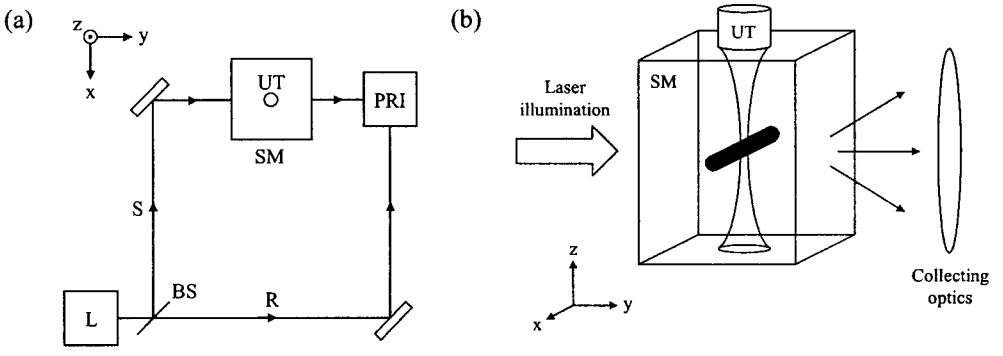


Figure 1 (a) Schematic diagram of the setup for the ultrasound-modulated optical imaging experiment. L: single-frequency laser source, BS: beam splitter, R: reference beam, S: signal beam, SM: scattering medium, UT: ultrasonic transducer, PRI: photorefractive interferometer. **(b)** Geometry of the scattering medium. The black cylinder is an optically absorbing object which is acoustically transparent.

Most results presented in the literature are obtained with low or moderate power single-frequency continuous-wave (cw) lasers of sufficiently long coherence length [2-7]. These sources limit the number of collectable photons at the exit of the scattering medium. With photorefractive interferometers, low power cw laser sources also lengthen the response time of the photorefractive crystal which becomes vulnerable to the speckle decorrelation induced by mechanical vibrations or by motions within the tissues for *in vivo* applications. For biomedical applications, a direct power scaling is not applicable since the maximum permissible exposure (MPE) in terms of average irradiance is rapidly reached in the visible and the near infrared parts of the spectrum (from $0.2\,W/cm^2$ to $1.0\,W/cm^2$). Power scaling is still attractive when considering the low sensitivity of ultrasound-modulated optical imaging due to a small tagged/untagged photons ratio and to the difficulty of collecting efficiently the photons at the exit of the scattering medium. An appropriate way to apply power scaling is the use of a source emitting a low duty cycle train of powerful laser pulses. Such a laser source can be obtained by amplifying a single-frequency cw laser beam with a flashlamp-pumped gain-switched amplifier. In the following sections, we described the components of an experimental setup based on such a pulsed laser.

2.1 Pulsed laser source

In our experiment, a cw single-frequency laser beam of 200 mW at 1.064 μm is provided by a commercial Nd:YAG non planar ring oscillator. This master oscillator (MO) is followed by the gain-switched amplifier depicted in Fig. 2(a). The linearly polarized laser beam of the master oscillator is transmitted through a first optical isolator (OI1) to prevent feedback from the amplifier. The amplifier is composed of two Nd:YAG laser rods (LR1-2) pumped by a single flashlamp (FL) which is powered by a variable pulse width flashlamp controller. The first laser rod (LR1) is used as a two-pass amplifying medium. The counter-propagating beams are separated by a quarter-wave plate (QW) followed by a thin film polarizer (TFP). An optical isolator (OI2) located between the two laser rods prevents the self-oscillation of the amplifier. The third amplifying pass occurs in the second laser rod (LR2). In typical operating conditions, 530-μs pulses of 280 mJ are obtained at a repetition rate of 25 Hz . Consequently, the overall gain, including the passive losses in the optical components, is higher than 2500. The gain in the third pass is typically around 5, indicating that gain saturation is almost reached. A typical pulse intensity profile at the output of the amplifier is shown in Fig. 2(b) where the peak power is higher than 500 W . Considering the repetition rate of 25 Hz , this corresponds to an average power of approximately 7 W . The use of counter-propagating orthogonal polarizations in the first laser rod minimizes the depolarization in the first two passes. The amplified output beam is partially depolarized by the thermal birefringence in the second laser rod of the amplifier. The output beam degree of polarization is typically of 0.8.

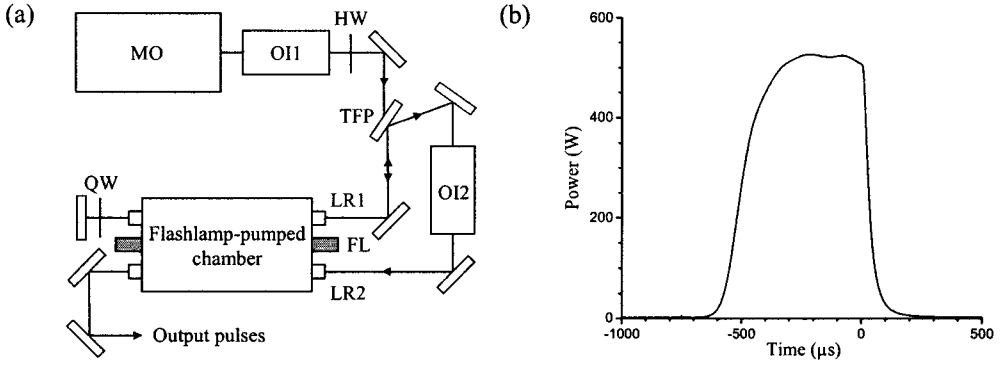


Figure 2 (a) Layout of the Nd:YAG amplifier. MO: 200-mW master oscillator, OI1-2: optical isolators, LR1-2: Nd:YAG laser rods (φ = 3 mm, L = 100 mm), FL: flashlamp, HW: half-wave plate, QW: quarter-wave plate, TFP: thin-film polarizer. Other components are plane dielectric mirrors **(b)** Typical output pulse intensity profile.

2.2 Characterization of the ultrasonic beam and the scattering medium

In order to use a scattering medium with an optical absorption coefficient μ_a comparable to that of water in the therapeutic window, we have used a liquid optical phantom based on sunflower oil. The optical absorption of sunflower oil at 1.064 μm was measured to be 3.2×10^{-3} mm^{-1}. As the optical scatterer, we have used titanium dioxide particles (DuPont Ti-PURE R-900, medium particle size: 0.41 μm). In our experiment, the scattering medium was insonified by a 4.35-MHz transducer with an active diameter of 6 mm. The transducer was fed with sinusoidal bursts produced by an arbitrary waveform generator and amplified by a high power amplifier. Such a transducer does not provide an optimum lateral resolution but the ultrasonic beam is well collimated over the probed distance.

In a first step, the ultrasonic beam produced by the transducer was calibrated by using the setup shown in Fig. 3(a). The ultrasonic transducer (UT) is immersed in sunflower oil (SO) and points toward the free oil-air interface. Assuming that the "particle" displacement is essentially longitudinal (along the axis z) as for almost plane waves, the ultrasonic beam (UB)

can be probed by measuring the displacement ξ_2 (as a function of time) of the oil-air interface with a broadband (10kHz–35MHz) heterodyne interferometer (HI) that uses the Fresnel reflection of the optical probe beam (PB) on the interface. The particles displacement ξ_1 associated with the progressive wave propagating in sunflower oil toward the free interface can be deduced from ξ_2 with the relationship $\xi_2 = \tau\xi_1$ where $\tau = 2Z_1/(Z_1+Z_2)$ is the displacement transmission coefficient, $Z_1 = 1.34\times10^6$ N·s/m^3 and $Z_2 = 0.41\times10^3$ N·s/m^3 being the acoustic impedances of sunflower oil and air. The pressure wave p_1 in sunflower oil is then calculated according to the relation $p_1 = Z_1 v_1$ where $v_1 = \partial\xi_1/\partial t$ is the particle velocity [14]. When compared to hydrophone measurements, this method provides a high spatial resolution, a simple calibration and a broadband detection. A typical displacement waveform $\xi_2(t)$ is shown in Fig. 3(b) with the corresponding pressure waveform $p_1(t)$. By following this procedure, the ultrasound field can be mapped without readjusting the probe beam by moving the transducer in sunflower oil with an xyz translation stage.

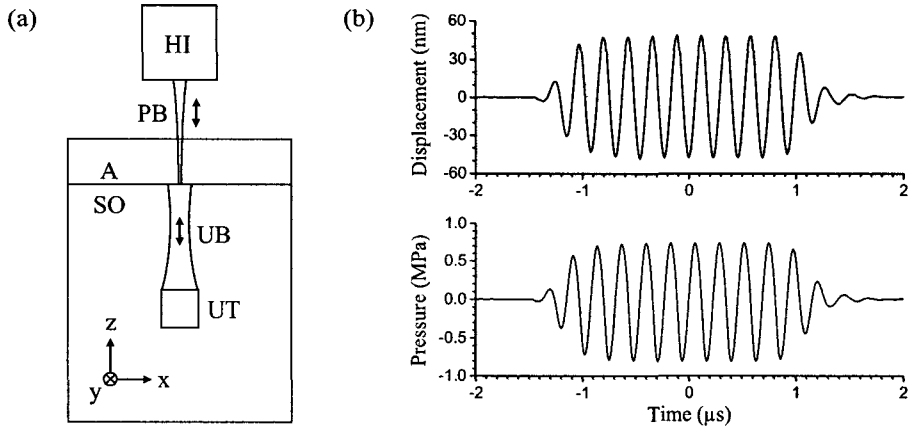


Figure 3 (a) Layout of the setup used to calibrate the ultrasonic pressure wave. SO: sunflower oil, A: air, UT: ultrasonic transducer, UB: ultrasonic beam, PB: probe beam, HI: heterodyne interferometer. **(b)** Typical calibrated displacement of the interface and the corresponding ultrasonic pressure wave in sunflower oil for a 10-cycle toneburst.

The natural focus of the acoustic field of a plane transducer is located at the so-called near-field distance $N = D^2/(4\lambda) \cong 27$mm where $D = 6.00$mm is the diameter of the transducer and $\lambda = 0.336$mm is the ultrasound wavelength at 4.35MHz [15]. By using the optical technique described above, the ultrasonic beam was characterized in the transverse plane at the near field distance. The result is shown in Fig. 4(a) in terms of average intensity (during the toneburst). The integrated average power in this plane was 3.7 W. Measurements carried out in three other transverse planes have confirmed an acoustic (intensity) losses coefficient $\alpha = 0.29\,\text{cm}^{-1}$. This value is in good agreement with the expression $\alpha = 16\pi^2\eta f^2/(3\rho c^3)$ where f is the frequency (4.35 MHz) and the properties of sunflower oil are: the viscosity $\eta = 0.08$Pa·s, the density $\rho = 0.92$g/cm^3 and propagation speed of sound $c = 1.46$mm/μs. The on-axis pressure was also measured and the axial profile shown in Fig. 4(b) presents, as expected, a local maximum approximately located at the near-field distance. The refractive index modulation associated with the propagation of the pressure wave is proportional to the the piezo-optic constant $\partial n/\partial p$ of the liquid. The piezo-optic constant of sunflower oil was measured by using a technique similar to that of Royer *et al.* [16]. We have obtained $\partial n/\partial p = 2.5\times10^{-10}\,\text{Pa}^{-1}$. This value is higher than that of more usual water-based optical phantoms for which $\partial n/\partial p = 1.5\times10^{-10}\,\text{Pa}^{-1}$ [17].

In our experiment, we have used an optical phantom composed titanium dioxide particles dispersed in sunflower oil. The extinction coefficient μ_t of this scattering medium was obtained by the collimated beam transmission method [1], that is, by measuring the ballistic transmission of a 20-mm thick cell as a function of the scattering medium concentration C

in pure sunflower oil. We obtained $\mu_t = 6\,\mathrm{mm}^{-1}$ from the fit with $I(C) = I_0 \exp(-\mu_t TC)$ where T is the thickness of the cell. According to the relation $\mu_t = \mu_s + \mu_a$, the absorption coefficient $\mu_a = 3.2\times10^{-3}\,\mathrm{mm}^{-1}$ of sunflower oil is negligible in the determination of the scattering coefficient μ_s. Consequently, the scattering mean free path l_s of our phantom was approximately of $170\,\mu\mathrm{m}$ at a wavelength of $1.064\,\mu\mathrm{m}$. This value is of the same order of magnitude than that of biological tissues at visible wavelengths (100 μm). It should be noted, however, that the absorption coefficient μ_a of sunflower oil at $1.064\,\mu\mathrm{m}$ is still higher than that of water in the visible ($3.2\times10^{-5}\,\mathrm{mm}^{-1}$ at 532 nm) and in the near infrared ($2.0\times10^{-3}\,\mathrm{mm}$ at 800 nm) [18-19].

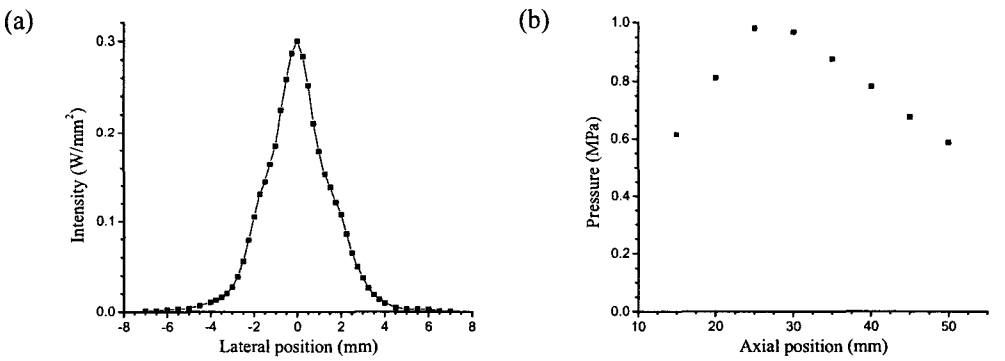


Figure 4 (a) Lateral intensity profile of the acoustic beam in the plane at the near field distance of the transducer in sunflower oil. **(b)** Measured on-axis pressure profile.

2.3 Adaptative interferometer

In ultrasound-modulated imaging, the design of the photorefractive interferometer must be adapted when considering the very low light level collected at the output of the scattering medium. The light gathering efficiency must be enhanced by maximizing the optical etendue of the interferometer. The scattering of the pump beam toward the axis of propagation of the signal beam must be minimized by using a configuration with orthogonal signal and reference beams [7]. Finally, a differential detection is preferable to eliminate the non negligible DC photocurrent over which the tagged-photon signal is superposed. In our experiment, the photorefractive interferometer was based on a GaAs crystal used in diffusion regime (no voltage applied). The layout of the interferometer is schematically shown in Fig. 5. The crystal is oriented so that the signal and reference beams enter respectively by the (110) and the $(1\bar{1}0)$ faces, both beams being polarized along the ⟨001⟩ axis. This corresponds to an anisotropic configuration with the grating vector oriented along the ⟨010⟩ axis. Special attention was paid to the optical etendue of the interferometer by using large numerical aperture ($NA = 0.54$) aspheric lenses with effective focal lengths $EFL = 20\,\mathrm{mm}$ and large active diameter ($\varphi = 3\,\mathrm{mm}$) InGaAs photodetectors. The optical etendue of the interferometer is determined by the surface S of the photodiodes ($7\,\mathrm{mm}^2$) and the numerical aperture of the aspheric lenses which corresponds to an acceptance solid angle Ω of $\sim 1\,\mathrm{sr}$. Consequently, the optical etendue of the interferometer was approximately equal to $7\,\mathrm{mm}^2\mathrm{sr}$. A near infrared liquid light guide (LLG) was used to carry the signal beam from the scattering medium to the input of the photorefractive interferometer. This LLG was the slightly limiting component of the setup with an optical etendue of $6.4\,\mathrm{mm}^2\,\mathrm{sr}$. Within the interferometer, the diverging beam exiting from the LLG is first collimated with an aspheric lens and polarized with a thin sheet polarizer. A second aspheric lens images the tip of the LLG on the entrance face of the GaAs crystal. The signal beam at the output of the crystal (C) is then collimated and sent through a half-wave plate (HW) followed by a polarizing beam splitter (PBS). Each polarization is then focused on a photodiode of the balanced receiver (BR). It should be noted that the transverse intensity profile of the reference beam was reshaped with cylindrical lenses

to obtain an elliptical beam matching more precisely the rectangular lateral face (10 mm x 7 mm) of the GaAs. This ensures an efficient use of the reference beam energy over the crystal length while minimizing the parasitic reflections.

Even with orthogonal signal and reference beams, the reference beam scattering and the parasitic reflections are responsible of a non negligible part of the energy impinging on the photodetectors. This is due to the difficulty of collecting efficiently the photons at the exit of the scattering medium. To minimize the DC component of the photocurrent that needs to be amplified, a differential configuration was used. The half-wave plate was adjusted to balance the illumination on both detectors. Such a compensation of the optical illumination almost eliminates the DC photocurrent before its amplification by the transimpedance amplifier, and that, without canceling the tagged-photon signal.

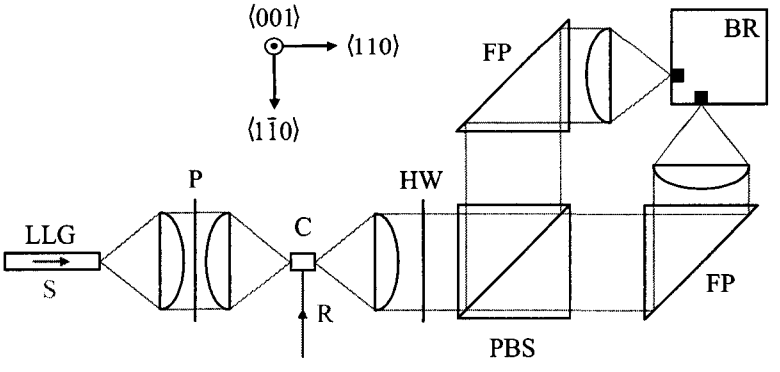


Figure 5 Layout of the photorefractive interferometer. S: signal beam, R: reference beam, C: GaAs crystal, LLG: liquid light guide, P: thin sheet polarizer, HW: half-wave plate, PBS: polarizing beam splitter, FP: folding prisms, BR: balanced receiver using two InGaAs photodiodes (φ = 3 mm). Other components are aspheric lenses (φ = 25 mm, EFL = 20 mm).

3. Results

In our setup (see Fig. 1), a variable beam splitter composed of a polarizing beam splitter cube and a half-wave plate was used to separate the reference and the signal beams. The signal beam was directed toward the scattering medium. The outgoing photons were coupled in the photorefractive interferometer through the liquid light guide which was directly butted against the rear face of the cell containing the scattering medium without any other collecting optics.

All the measurements were carried out in conditions allowed by the biomedical safety limits [8-9]. The mechanical index (MI) of an ultrasonic wave is given by the ratio $P/\sqrt{f}$ where P is the maximum rarefraction pressure (in MPa) and f is the ultrasound frequency (in MHz). In our experiment, the maximum negative pressure was typically around 1 MPa corresponding to MI=0.5. This value well below the safety limit (MI=1.9). Moreover, at a wavelength of 1.064 μm, the laser beam irradiance must be maintained below a maximum permissible exposure (MPE) of 1.0 W/cm^2. In our experiment, the scattering medium was typically illuminated on a 30-mm diameter surface with 60-mJ pulses at a repetition rate of 25 Hz. Consequently, the average irradiance was approximately equal to 200 mW/cm^2. This value is equal to the MPE in the visible and is 5 time more stringent than the MPE at our working wavelength of 1.064 μm.

The first measurements were obtained with a well controlled scattering medium composed of titanium dioxide particles dispersed in sunflower oil. The concentration of titanium dioxide particles was adjusted to get a reproducible scattering mean free path of 170 μm and the scattering medium thickness (along the axis y) was equal to 30 mm.

3.1 Properties of the tagged-photon signal

The tagged-photon signal obtained with the GaAs photorefractive interferometer was first characterized as a function of the ultrasonic excitation of the scattering medium. With the anisotropic configuration of the photorefractive interferometer considered here, a quadratic response with the optical phase modulation amplitude is expected. Figure 6(a) shows the tagged-photon signals as a function of time for different pressure wave amplitudes. These signals were obtained with 10-cycle acoustic bursts at 4.35 MHz. Figure 6(b) shows the corresponding maximums of the tagged-photon signals as a function of the amplitude of the pressure wave. As expected, the increase of the tagged-photon signal is quadratic with the applied pressure.

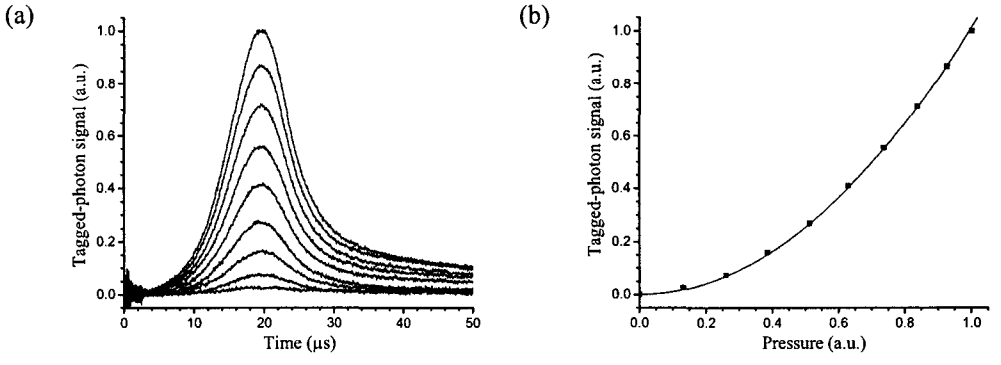


Figure 6 (a) Tagged-photon signals as a function of time obtained with 10-cycle tonebursts of different pressure wave amplitudes. **(b)** Corresponding maximums of the tagged-photon signals as a function of the pressure wave amplitude. The curve is a parabolic fit with the experimental points.

The use of ultrasonic tonebursts provides an axial resolution (along the axis z) given approximately by $\Delta z = c\Delta t$ where Δt is the duration of the toneburst and c is the speed of sound in the scattering medium. With very short tonebursts (few cycles in the MHz frequency range), the spatial resolution along the ultrasonic axis z can be of the order of 1 mm. However, the insonified volume decreases linearly with the number of cycles which leads to a reduction of the tagged-photon signal. Consequently, a compromise must be done between the signal level and the spatial resolution along the ultrasound axis.

Figure 7(a) shows the tagged-photon signal as a function of time by using pressure waves of the same amplitude but containing different number of acoustic cycles at 4.35 MHz. These curves were obtained with 2^n acoustic cycles where n = 0 (1 cycle) for the lower curve and n = 7 (128 cycles) for the upper curve. The amplitude and the duration of the signal both increase with the number of acoustic cycles. Figure 7(b) shows the corresponding maximums of the tagged-photon signals as a function of the number of acoustic cycles. For a small number of acoustic cycles – corresponding to an insonified zone much shorter than the zone probed by the collecting optics – the signal level increases almost linearly with the number of acoustic cycles. This behavior is expected by the fact that the insonified volume also increases linearly with the number of acoustic cycles in this limiting case. As mentioned above, this signal enhancement is made at the cost of a lost of resolution along the axis z. A saturation of the signal level is reached when the ultrasonic toneburst duration corresponds to a spatial extent (along the axis z) similar to the lateral extent of the volume probed by the collecting optics.

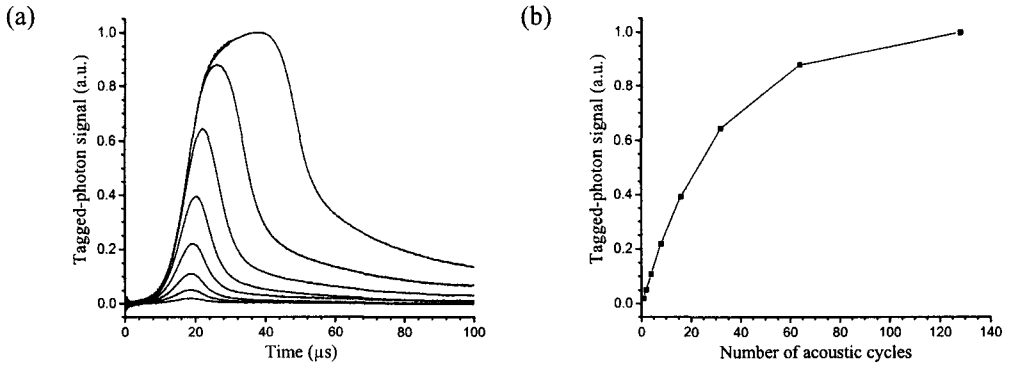


Figure 7 (a) Tagged-photon signals as a function of time obtained with tonebursts of the same pressure but with 2^n acoustic cycles (n=0: lower curve, n=7: upper curve). **(b)** Corresponding maximums of the tagged-photon signals as a function of the number of acoustic cycles.

3.2 Absorbing object detection in a 30-mm thick scattering medium

In envisioned biomedical applications, the optically absorbing object is often expected to be acoustically matched to the surrounding medium. In our experiment, we have used a thin polyester (Mylar) tube with wall thickness of 12.7 μm. The wall thickness of the tube was sufficiently thin to be acoustically transparent [14,16]. The tube was 50-mm long and held at both extremities with an aluminum holder. The tube was filled with sunflower oil. The level of scattering inside the tube was adjusted by adding titanium dioxide particle and the level of optical absorption was adjusted by adding smocked black.

Different propagation regimes exist from ballistic to scattering. Since the evaluation of the scattering coefficient μ_s and the anisotropy factor g is not always straightforward, a simple test is useful to verify whether the propagation regime is ballistic, scattering or in between. By definition, ballistic and quasi-ballistic photons cross the medium without significant deviation from their rectilinear path. Standard optical imaging is still applicable with these photons. A simple test to determine if the ballistic contribution is non-negligible consists in positioning the absorbing object in front of the insonified zone, within the incident laser beam. If the propagation is essentially ballistic, a local drop will be observed on the tagged-photon signal as a function of time. This would be a result of a geometrical optical shadow effect. On the contrary, if the propagation is truly scattering, the presence of an object in front of the insonified zone will have no localized effect on the tagged-photon signal. In this case, a local drop of the signal is observable only when the absorbing object is located in the insonified zone.

Figure 8 shows the results obtained with the scattering medium ($l_s = 170\mu m$) described in section 2.2 enclosed in a 30-mm thick cell of Plexiglas. The transverse dimensions of the cell were 60 mm along the axis x and 90 mm along the axis z. The laser beam and the liquid light guide were both centered at ~30 mm below the transducer. The scattering medium was insonified with 10-cycle tonebursts of 4.35 MHz. Figure 8(a) was obtained with a 5.3-mm absorbing cylinder located in the insonified zone as shown in Fig. 1(b). The distance between the cylinder and the transducer was approximately equal to the near-field distance of the acoustic beam (27 mm). A local decrease of the tagged-photon signal level is clearly observed around t = 20 μs corresponding to the time of propagation of the toneburst between the transducer and the object. The tagged-photon signal does not drop to zero since the absorbing object diameter is slightly inferior to the acoustic beam diameter shown in Fig. 4(a). When considering the cylinder diameter of 5.3 mm, one may first expect a signal drop duration approximately equal 3.6 μs plus the duration of the toneburst (2.3 μs). In fact, the duration of the signal drop is slightly superior to this value because the photons propagating in the neighborhood of the absorbing object are also more likely to be absorbed when following their scattering path. In ultrasound-modulated imaging, this effect could lead to a slight

degradation of the reconstructed image sharpness. Figure 8(b) was obtained with the same absorbing cylinder in front of the insonified zone. In this case, the absorbing object does not lead to any local decrease of the tagged-photon signal indicating a truly scattering propagation regime (no geometrical shadow effect).

It should be noted that the lower traces in Figs. 8(a) and (b) were obtained with a single pulse, that is, without averaging. The use of a pulsed laser has also allowed obtaining photorefractive crystal response time shorter than the speckle decorrelation time associated with mechanical vibrations. Consequently, the measurements shown here were done without having to use any vibration isolation technique.

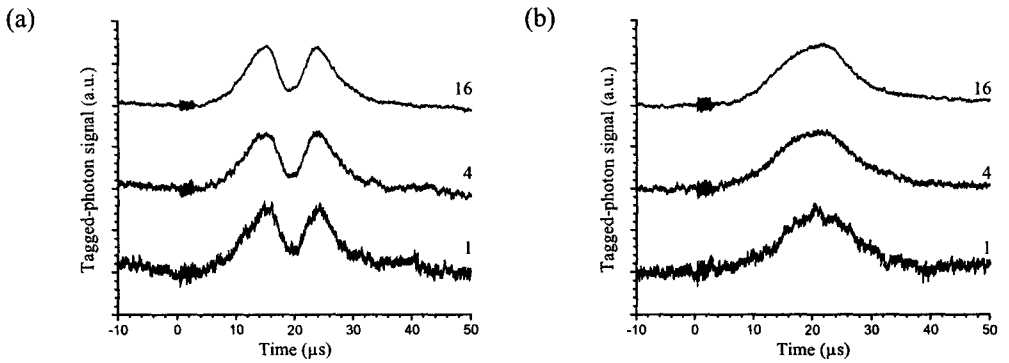


Figure 8 (a) Tagged-photon signal with a 5.3-mm diameter cylindrical absorbing object in the insonified zone. **(b)** Corresponding signals when the absorbing object is located in front of the insonified zone. In (a) an (b), the number of pulses used to average the signal is indicated aside each curve.

In ultrasound-modulated optical imaging, one expects to be able to measure the size and the location of the absorbing object as well as its optical contrast with the surrounding medium at the probing wavelength. Both aspects are considered in Fig. 9. In Fig. 9(a), two highly absorbing cylinders of 3.3- and 5.3-mm diameters were successively placed in the insonified zone. The red curve obtained with the 3.3-mm cylinder shows a signal drop of shorter duration and lower visibility than the blue curve obtained with the 5.3-mm diameter cylinder. The change of duration is due to the difference in diameter while the change of visibility is due to the different ratios between the objects diameters and the ultrasound beam diameter.

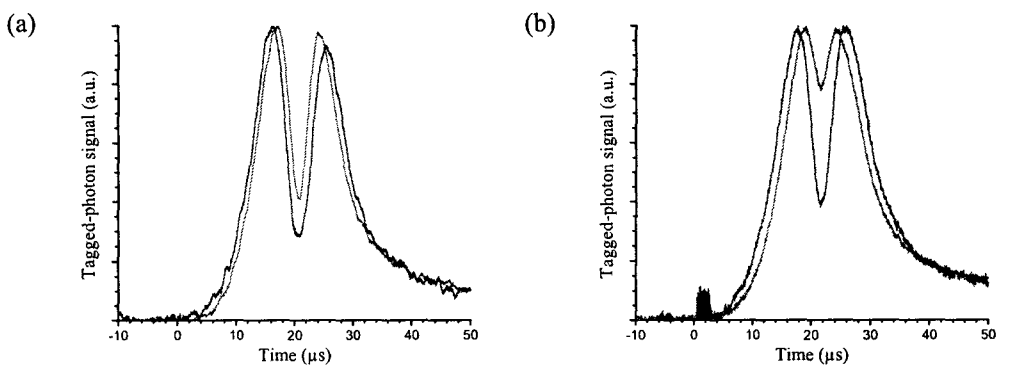


Figure 9 (a) Detection of a cylindrical absorbing object in the insonified zone with a diameter of 3.3 mm (red line) and 5.3 mm (blue line). **(b)** Detection of a 4.3-mm diameter cylindrical object with a low optical absorption (red line) and high optical absorption (blue line).

In Fig. 9(b), two cylinders of 4.3-mm diameters were used, the difference between both objects being the level of absorption. The red curve was obtained with a slightly absorbing cylinder. In this case, the polyester tube was filled with the scattering medium to which was added a light concentration of smocked black giving a very light grey appearance to the object. The blue curve was obtained with a highly absorbing cylinder (black appearance). The optical contrast is clearly observed by the depth of the signal drop but the duration of the signal drop is also affected by the level of absorption. As mentioned earlier, the level of absorption also influences the effective dimension of the objet since the surrounding scattering photons are more likely to be absorbed when propagating in the neighborhood of a highly absorbing object.

3.3 Tagged-photon signals in a 60-mm thick scattering medium

Measurements described in section 3.2 were obtained with a single pulse by using a short acoustic burst (10 cycles) in a 30-mm thick scattering medium. In this section, we describe measurements performed using the same scattering medium enclosed in a 60-mm thick Plexiglass cell.

The first series of measurements was done with 10-cycle acoustic bursts in order to compare the lateral extent (along x and y axes) of the volume optically probed by the liquid light guide. The transverse profile of the tagged-photon signal along the axis x was obtained by translating the transducer over the scattering medium. The maximums of the tagged photon signals for each position x is given by the series of red points in Fig. 10(a). Considering the cylindrical symmetry of the photon migration around the axis y, lateral extent of the tagged-photon signal along the axis z should be similar. However, along the axis z, the measurement is done as a function of time without moving the transducer. The temporal to spatial mapping is then simply given by $z = ct$ where $c = 1.46\,\text{mm}/\mu s$. The curve obtained in this way is shown in Fig. 10(a) and confirm the cylindrical symmetry of the photon migration. Is should be noted that, with this 60-mm thick scattering medium, the signal-to-noise ratio obtained with 10-cycle acoustic bursts wasn't sufficiently high to allow measurements with a single pulse. Averaging with 512 pulses was used in this case.

The detection of a 5.3-mm diameter absorbing cylinder was also performed in the 60-mm thick scattering medium. The results obtained with (red line) and without (black line) the absorbing cylinder are compared in Fig. 10(b). Again avering with 512 pulses (corresponding to 20 seconds) was necessary to obtain a good signal-to-noise ratio.

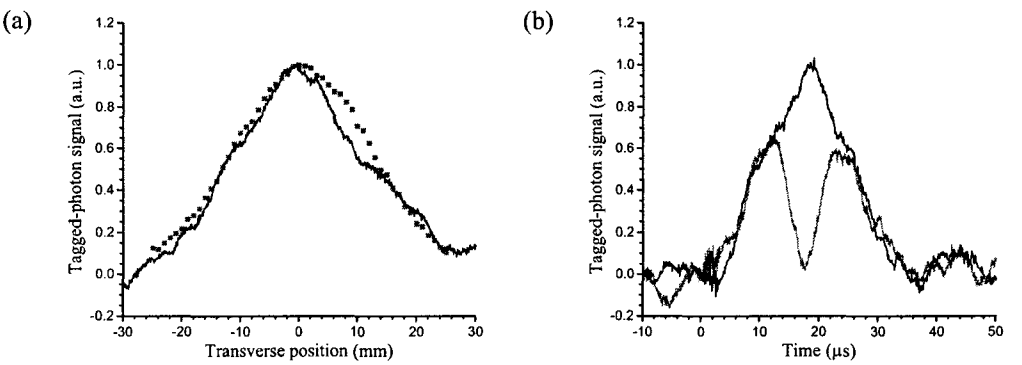


Figure 10 Tagged-photon signals obtained in a 60-mm thick scattering medium using 10-cycle acoustic bursts. **(a)** The red points were obtained by translating the transducer along the axis x and the black curve was obtained from a temporal to spatial mapping along the axis z. **(b)** Signals obtained with (red line) and without (black line) an optically absorbing cylinder of 5.3 mm diameter.

An alternative approach to obtain a three-dimensional reconstruction of an absorbing object embedded in a scattering medium is the tomographic reconstruction. In this approach, long acoustic bursts can be used to enhance the signal level since the resolution along the ultrasound axis is no more obtained by a temporal to spatial mapping. By using acoustic bursts of 100 cycles, we were able to obtain single shot measurement of tagged photons. Signals obtained with 1, 4 and 16 pulses are presented in Fig. 11.

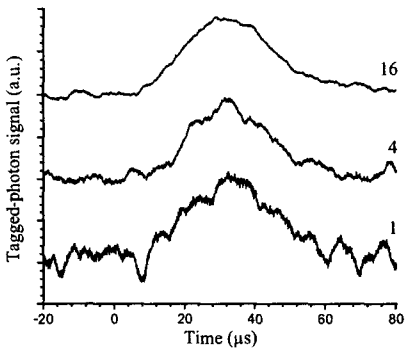


Figure 11 Tagged-photon signals obtained in a 60-mm thick scattering medium by using 100-cycle acoustic bursts. The number of pulses used to average the signal is indicated aside each curve.

3.4 Measurements in 30- and 60-mm thick samples of chicken breast

Measurements in optical phantoms are useful to control and to get reproducible scattering and absorption properties. However, the use of animal tissues is closer to the envisioned biomedical applications. Consequently the next measurements were performed using chicken breasts as the scattering medium. As for the preceding results, all the following measurements were carried out in conditions allowed by the biomedical safety limits, the mechanical index being approximately equal to 0.45 and the laser beam average irradiance being equal to 200 mW/cm^2. The signal collection was again accomplished with the LLG directly butted against the rear side of the Plexiglas cell.

For the first measurements, an appropriately cut chicken breast was slightly compressed in a 30-mm thick Plexiglas cell (60 mm x 90 mm in the transverse dimensions). The chicken breast filled rather well the upper 60 mm of the cell. The rest of the cell was filled with sunflower oil and the coupling between the ultrasonic transducer and the chicken breast was accomplished with a thin layer of sunflower oil. A black rubber inclusion of 6x6x4 mm^3 was added inside the chicken breast, in the plane approximately located at 15 mm from the front and the back surface of the cell. The detection of this absorbing object was performed by moving the ultrasonic transducer along the axes x and y until a local drop in the tagged-photon signal was observed. The results are shown in Fig. 12(a) as a function of the number of pulses used to average the signal. Short acoustic burst of 10 cycles (2.3 μs) were used to obtain these signals. The signal-to-noise ratio is clearly acceptable even with a single pulse (lower trace). It should be note that no local decrease of signal was observable on the traces when the absorbing object was located in front of the scattering medium (instead of inside). This indicates that the local decrease was not the result of a shadow effect. These results also confirm that the calibrated scattering medium used in previous sections was representative of more realistic samples like chicken breasts.

For the second measurements, two chicken breasts were gently compressed together in a 60x60x90 mm^3 Plexiglas cell. The chicken breasts filled rather well the upper 60 mm of the cell. Again, the rest of the cell was filled with sunflower oil and the coupling between the ultrasonic transducer and the chicken breast was accomplished with a thin layer of sunflower oil. In this case, a black rubber inclusion of 6x6x5 mm^3 was added between the two chicken

breasts, approximately in the plane located at 30 mm from the front and the back surface of the cell. The detection of this absorbing objet was performed by moving the ultrasonic transducer along the axes x and y until a local drop in the tagged photon signal was observed. With such a thick sample, a good signal-to-noise ratio was obtained by averaging with 512 pulses (20 seconds measurement). The results obtained with acoustic bursts of 10 and 20 cycles are shown in Fig. 12(b). As expected, the amplitude of the tagged-photon signal is higher with longer acoustic burst but the visibility of the absorbing object is then reduced. To our knowledge, this is the first measurement made in such a thick scattering medium. It should be noted that the signal-to-noise ratio was limited by the Johnson noise which means that a better design of the balanced receiver could lower the number of pulses needed to average the signal. The use of an acoustic wave with the maximum amplitude allowed by safety limits (MI = 1.9 instead of 0.5) would have been sufficient to obtain almost single-shot measurements (with the same signal-to-noise ratio) or to enhance the spatial resolution by focusing the acoustic beam. Further improvement could also be made by reducing the laser pulse duration in order to increase the repetition rate while remaining below the MPE.

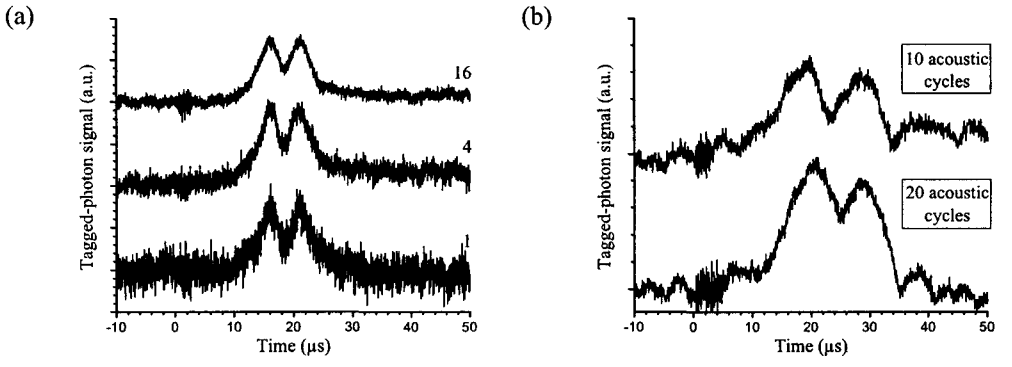


Figure 12 (a) Tagged-photon signals obtained in a 30-mm thick chicken breast by using 10-cycle acoustic bursts. The absorbing object was a black rubber inclusion (6x6x4 mm^3). Each curve is identified with the number of pulses used to average the data. **(b)** Tagged-photon signals obtained in a 60-mm thick sample of chicken breast by using 10-cycle (upper trace) and 20-cycle (lower trace) acoustic bursts. The absorbing object was a black rubber inclusion (6x6x5 mm^3). Each curve was obtained by averaging with 512 pulses.

4. Conclusions

The work presented herein has shown that a pulsed laser source with a long coherence length can be implemented by using a flashlamp-pumped gain-switched amplifier at the output of a single-frequency cw laser. A low duty cycle pulse train with high peak power concentrates the illumination of the scattering medium mainly during the transit time of the acoustic pulse while maintaining the average power below the maximum permissible exposure. A high peak power also increases the available power density to reduce the response time of the dynamic hologram written in the photorefractive crystal of the adaptative interferometer. In the pulsed laser scheme considered here, a short response time is essential to write the grating in a timescale shorter than the laser pulse duration. In addition, a short response time ensures to obtain a setup immune to mechanical vibrations and to the short speckle decorrelation time encountered in vivo.

Adaptative photorefractive interferometer based on a GaAs crystal was used to detect ultrasound-modulated photons. Special care was taken to increase the optical etendue of the interferometer by using large area InGaAs detectors and high numerical aperture aspheric lenses. The use of a liquid light guide has allowed an efficient collection of the scattered photons without limiting significantly the optical etendue of the setup.

The spatial resolution along the ultrasound axis was obtained by using few-cycle acoustic bursts. Tagged-photon signals were obtained in a truly scattering propagation regime without going beyond the biomedical safety limits in terms of ultrasonic wave amplitude and laser beam irradiance. The detection of an optically absorbing object in a 30-mm thick scattering medium was performed without averaging with 10-cycles acoustic bursts at 4.35 MHz. Tagged-photons signals were also obtained without averaging in 60-mm thick scattering medium by using 100-cycle acoustic bursts. Similar results were obtained by using chicken breast samples as the scattering medium. In this case, a measurement with a single pulse was demonstrated in a 30-mm thick sample. By allowing averaging with 512 pulses, an absorbing object of 6x6x5 mm^3 was detected inside a 60-mm thick sample of chicken breast. The use of an acoustic wave with the maximum amplitude allowed by safety limits would have been sufficient to obtain almost single-shot measurements with the same signal-to-noise ratio or to enhance the spatial resolution.

The results presented here demonstrate the pertinence of a high power laser source to allow the detection of optically absorbing objects in very thick scattering media by using ultrasound-modulated optical imaging. With such a laser source, this can be accomplished without being affected by speckle decorrelation, an essential requirement for biomedical applications were mechanical vibrations and movements within the scattering medium cannot be eliminated.